PREDICTION OF THE FLOW OVER A THIN FLAT PLATE AT SHALLOW INCIDENCE

André Luiz Tenório Rezende, arezende@mec.puc-rio.br
Angela Ourivio Nieckele, nieckele@mec.puc-rio.br
Department of Mechanical Engineering, PUC/Rio, 22453-900, Rio de Janeiro, RJ, Brazil

Abstract. *The numerical simulation of the flow over a thin flat plate at low incidence angles is the focus of this study. The numerical prediction of this complex flow presents a significant challenge due to the presence of laminar-to-turbulent transition, boundary layer separation and reattachment. The principal interest is the formation of the thin and long leading edge bubble due to the flow separation at the sharp leading edge. The numerical solutions are obtained through the Reynolds Averaged Navier-Stokes (RANS) equations for the two-dimensional steady state flow, using the Spalart-Allmaras and SST turbulence models. Simulations were accomplished for inclination angles of the flat plate from 1 to 5 degrees with a Reynolds number of 2.13 × 10^5. The results are compared with available wind tunnel experimental data.*

Keywords*: flat plate, shallow incidence angle, RANS, reattachment*.

1. INTRODUCTION

The understanding of the flow around thin flat plate at shallow incidence can help in the design of airfoils and sails (Cyr, Newman, 1996), as well as flexible wing-based micro air vehicles (Lian and Shyy, 2005). The flow around an inclined flat plate with a sharp leading edge, as shown in Fig. 1, results in a long and thin bubble, denominated "thin aerofoil bubble" (Gault, 1957). At zero incidence angle, the stream is laminar and attached on both sides, generating zero lift (assuming equal surface profiles). If the plate has an incidence angle, the stagnation point moves to the inferior surface. The boundary layer around the leading edge is very thin, and it is expected to separate immediately, due to the flow direction change. The fixed separation point leads to the hypothesis that the flow will be insensitive to a change in Reynolds number, and transition will occur soon after separation.

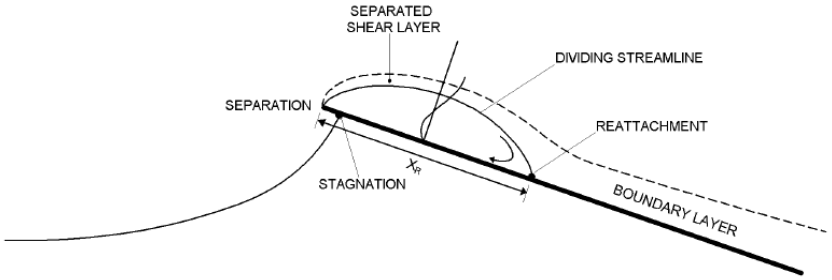

Figure 1. Simplified model of a thin aerofoil separation bubble.

The thin aerofoil bubble created on a plate with a sharp leading edge is consequently characterized by a flow separation at the leading edge with a consequent reattachment to the upper surface at a point which moves gradually downstream with increasing incidence. If the incidence angle is sufficiently small (usually smaller than 7 degrees), the flow reattaches. As shown in Fig. 1, there is a dividing streamline which demarcates the bubble from the outer flow and which rejoins the surface at the reattachment point. For greater angles, there is no reattachment point, the bubble enlarges downstream into the wake (Newman and Tse, 1992).

Subsequent to separation, a deficiency of viscous damping at the wall means that the shear layer is expected to suffer transition very close to the leading edge. The turbulent shear layer increases quickly and has a high entrainment rate; it then reattaches further downstream and bifurcates. Some flow is going to upstream to feed the shear layer and the resultant backflow reduces the pressure at the surface and in turn helps to bend the shear layer back to the reattachment point. The remaining flow is driven directed downstream where reverts gradually to an attached turbulent boundary layer before reaching the trailing edge (assuming there to be enough length left after reattachment).

This complex flow around a plate at the shallow incidence has been experimentally investigated by Crompton (2001). Detailed velocity and turbulence statistics were measured in wind tunnel for the leading edge bubble with the use of Laser Doppler Anemometry (LDV) for inclination angles of the flat plate varying from 1 to 5 degrees with a Reynolds number chord of 2.13×10^5. Following the work of Crompton, numerical studies based on Reynolds Average Navier-Stokes methodology (RANS) with the κ–ω and SST models were developed by Collie (2005). Due to the inability of Reynolds Average models (RANS) to capture the strong anisotropy of this type of flow, Sampaio et al.

(2006a, 2006b) employed the Large-Eddy Simulation (LES) methodology to the same thin flat plate test case, with an incidence angle of one degree, aiming a better understanding of the physics involved. Although, better agreement with experimental data were obtained, the large cost involved in those simulations encouraged the investigation of the present work for different angles of attach with the RANS methodology. Further, the influence of the selection of different turbulence models is also addressed. The first model selected is the Spalart-Allmaras model (Spalart, Allmaras, 1992) that uses a differential equation for transport of the eddy viscosity. The other one is the Shear-Stress Transport (SST) κ–ω (Menter, 2003) that uses the best qualities of the models κ–ε and κ–ω through a blend function and had best results than κ–ω model in previous study developed by Collie (2005).

2. MATHEMATICAL MODEL

The Reynolds-averaged approach is based on decomposing the velocity as $\mathbf{u} = \overline{\mathbf{u}} + \mathbf{u}'$ where $\mathbf{u}$ is the average velocity vector and $\mathbf{u}'$ the velocity vector fluctuation. The average continuity and momentum equation (RANS), for a steady state incompressible flow is given by

$$\nabla \bullet \overline{\mathbf{u}} = 0 \quad ; \quad \nabla \bullet (\overline{\mathbf{u}}\, \overline{\mathbf{u}}) = - \nabla(\frac{p}{\rho}) + \upsilon \nabla^2 \overline{\mathbf{u}} + \nabla \bullet (- \overline{\mathbf{u}'\, \mathbf{u}'}) \tag{1}$$

where ρ is the density, $\upsilon=\mu/\rho$ is the cinematic viscosity, μ is the molecular viscosity, p is the pressure. Equation (1) has the same form of the Navier-Stokes equation, but now it has an additional term, the turbulent Reynolds stress term, $-\overline{\mathbf{u}'\, \mathbf{u}'}$, representing the influence of the fluctuation on the average flow. In order to close Eq. (1), the turbulent Reynolds stress can be modeled based on the Boussinesq hypothesis, where the turbulent stress is obtained through an analogy with Stokes law, i.e., the stress is proportional to the deformation rate. The turbulence models selected to be investigated at the present work are described next.

2.1. SST *k-ω* MODEL

The turbulent Reynolds stress is modeled as

$$-\overline{\mathbf{u}'\, \mathbf{u}'} = \upsilon_t (\nabla\, \overline{\mathbf{u}} + \nabla\, \overline{\mathbf{u}})^T - \frac{2}{3} \kappa\, \boldsymbol{\delta} \tag{2}$$

where κ is the turbulent kinetic energy and υ_t is the turbulence viscosity, which is defined in accordance with the Shear-Stress Transport (SST) κ–ω model (Menter, 2003). This model was proposed for aeronautical flows simulations with strong adverse pressure gradients and separation with the best behavior of the κ–ε and κ–ω models. For boundary layers flows, the κ–ω model is superior to the k-ε model in the solution of the viscous near-wall region, and has been successful in problems involving adverse pressure gradients. Nevertheless, the κ–ω model requires a non-zero boundary condition on ω for non-turbulent free-stream, and the calculated flow is very sensitive to the value specified (Menter, 1992). It has also been show (Cazalbou *et al* , 1993) that the κ-ε model does not suffer this deficiency.

Thus, the SST model blends the robust and precise formulation of the κ–ω model close to walls with the free-stream independence of the κ–ε model outside the boundary layer. To accomplish this, the κ–ε model is written in terms of ω. Then the standard κ–ω model and the transformed κ–ε model are both multiplied by a blending function and both models are added together. This blending function F_1 is zero (leading to the standard κ–ω model) at the inner edge of a turbulent boundary layer and blend to a unitary value (corresponding to the standard κ–ε model) at the outer edge of the layer. Therefore the turbulent kinetic energy κ and specific dissipation rate ω of the SST model is given by (Menter, 2003):

$$\frac{\partial \kappa}{\partial t} + \overline{u}_i \frac{\partial \kappa}{\partial x_i} = \widetilde{P}_\kappa - \beta^* \kappa\, \omega + \frac{\partial}{\partial x_j} \left[(\upsilon + \sigma_\kappa\, \upsilon_t) \frac{\partial \kappa}{\partial x_j} \right] \tag{3}$$

$$\frac{\partial \omega}{\partial t} + \overline{u}_i \frac{\partial \omega}{\partial x_i} = \alpha\, S^2 - \beta \omega^2 + \frac{\partial}{\partial x_j} \left[(\upsilon + \sigma_\omega\, \upsilon_t) \frac{\partial \omega}{\partial x_j} \right] + (1 - F_1)\, 2\, \sigma_d\, \frac{1}{\omega} \frac{\partial \kappa}{\partial x_j} \frac{\partial \omega}{\partial x_j} \tag{4}$$

The last term in right side of Eq. (4) is known as cross diffusion term. Menter (1992) demonstrated that introducing cross diffusion term in the ω equation, the freestream dependency of the κ–ω model is reduced. The main effect of cross diffusion in free-shear flows is to increase the production of ω, which consequently increases the dissipation of κ. In the Eq. (4) the cross diffusion is multiplying by blending function F_1 based upon the distance to the nearest wall. As

explained previously, F_1 is equal to zero in the far field (κ–ε model), and switches over to one inside the boundary layer (κ–ω model). The blending function F_1 is defined as

$$F_1 = \mathbf{tanh}\left(arg_1^4\right) \quad ; \qquad arg_1 = \mathbf{min}\left[\mathbf{max}\left(\frac{\sqrt{\kappa}}{\beta^* \omega\, y}; \frac{500\,\upsilon}{y^2 \omega}\right); \frac{4\,\rho\,\sigma_{\omega 2}\,\kappa}{CD_{\kappa\omega}\, y^2}\right] \tag{5}$$

where y is the distance to the nearest surface and $CD_{\kappa\omega}$ is the positive portion of the cross diffusion term, given for

$$CD_{\kappa\omega} = \mathbf{max}\left(2\,\rho\,\sigma_d\,\frac{1}{\omega}\frac{\partial\kappa}{\partial x_j}\frac{\partial\omega}{\partial x_j}; 10^{-10}\right) \tag{6}$$

The definition of the turbulent eddy viscosity provides a better treatment of the transport of turbulent shear-stress in adverse pressure gradient boundary layers. This definition is based on Bradshaw's hypothesis that in boundary layer flows the Reynolds shear stress is proportional to the turbulent kinetic energy. The turbulent eddy viscosity is formulated as follows:

$$\upsilon_t = \frac{a_1\,\kappa}{\mathbf{max}\left(a_1\,\omega\,;\, S\,F_2\right)} \tag{7}$$

where S is the modulus of the mean rate-of-strain tensor S_{ij},

$$S = \sqrt{2\;S_{ij}\;S_{ij}} \quad ; \quad S_{ij} = \frac{1}{2}\left(\frac{\partial\,\overline{u}_i}{\partial\,x_j} + \frac{\partial\,\overline{u}_j}{\partial\,x_i}\right) \tag{8}$$

and F_2 is the blending function for the turbulent eddy viscosity in the SST model, defined as

$$F_2 = \mathbf{tanh}\left(\mathbf{arg}_2^2\right) \quad ; \qquad \mathbf{arg}_2 = \mathbf{max}\left(\frac{\sqrt{\kappa}}{\beta^*\,\omega\,y}; \frac{500\,\upsilon}{y^2\omega}\right) \tag{9}$$

In the SST model the production of turbulence kinetic energy is limited to prevent the build-up of turbulence in stagnation regions as

$$\widetilde{P}_k = \mathbf{min}\left(\upsilon_t\;S^2\;; 10\beta^*\kappa\;\omega\right) \tag{10}$$

Let ϕ represent the set of closure constants for the SST model and let ϕ_1 and ϕ_2 represent the constants from the standard κ–ω and κ–ε models respectively. The constants ϕ are calculated using a blend between the constants ϕ_1 (κ–ω) and ϕ_2 (κ–ε), which can be seen in Table 1, as

$$\phi = F_1\phi_1 + (1 - F_1)\phi_2 \tag{11}$$

Table 1. Closure coefficients of the SST model.

	β	$\beta*$	σ_κ	σ_ω	σ_d	α
ϕ_1 (standard κ–ω)	0.075	0.09	0.5	0.5	0.856	5/9
ϕ_2 (standard κ–ε)	0.0828	0.09	1.0	0.856	0.856	0.44

2.2. SPALART-ALLMARAS MODEL

Developed by Spalart and Allmaras (1992), this is a model relatively simple that solves a transport differential equation for the turbulent viscosity and, therefore, it requests smaller computational effort. The Spalart-Allmaras model was designed specifically for aerospace applications involving wall-bounded flows and adverse pressure gradients. The

differential equation is derived by using empiricism, arguments of dimensional analyses and selected dependence on the molecular viscosity. For this model, the turbulent Reynolds stress is modeled without the last term of Eq. (2), as

$$-\overline{\mathbf{u}'\ \mathbf{u}'} = \upsilon_t (\nabla\ \overline{\mathbf{u}} + \nabla\ \overline{\mathbf{u}})^T . \tag{12}$$

The eddy viscosity is defined as

$$\upsilon_t = \tilde{\upsilon}\ f_{v1} \tag{13}$$

where $f_{\upsilon l}$ is a viscous damping function used to treat more appropriate the buffer layer and viscous sublayer, computed as

$$f_{v1} = \frac{\chi^3}{\chi^3 + C_{v1}^3} \quad ; \quad \chi \equiv \frac{\tilde{\upsilon}}{\upsilon} \tag{14}$$

The transport equation for the working variable $\tilde{\upsilon}$ is given by (Deck et al, 2002)

$$\frac{\partial \tilde{\upsilon}}{\partial t} + \frac{\partial (\bar{u}_i\ \tilde{\upsilon})}{\partial x_j} = G_v + \frac{1}{\sigma_{\tilde{v}}}\left\{\frac{\partial}{\partial x_j}\left[(\upsilon + \tilde{\upsilon})\frac{\partial \tilde{\upsilon}}{\partial x_j}\right] + C_{b2}\left(\frac{\partial \tilde{\upsilon}}{\partial x_j}\right)^2\right\} - Y_v \tag{15}$$

In the Eq. (15), G_υ is the production term. Dacles-Mariani *et al* (1995) combine the effects of the rotation and strain tensors in the definition of production of υ_t, in order to avoid overestimation of the turbulent viscosity, in regions where the vorticity measure exceeds the strain rate. G_υ is based on a modification on the vorticity magnitude Ω in order to maintains its log-layer behavior, where Ω_{ij} is the mean rate-of-rotation tensor.

$$G_v = C_{b1}\ \tilde{\Omega}\ \tilde{\upsilon} \quad ; \quad \tilde{\Omega} = \Omega + \frac{\tilde{\upsilon}}{\kappa^2\ d^2}\ f_{v2} + C_{prod}\ \mathbf{min}\ (\ 0,\ S - \Omega\ ) \quad ; \tag{16}$$

$$\Omega_{ij} = \frac{1}{2}\left(\frac{\partial\ \bar{u}_i}{\partial\ x_j} - \frac{\partial\ \bar{u}_j}{\partial\ x_i}\right) \quad ; \qquad \Omega = \sqrt{2\ \Omega_{ij}\ \Omega_{ij}} \tag{17}$$

where d is the wall distance, C_{prod}=2.0 and f_{v2} is a damping function, given by

$$f_{v2} = 1 - \frac{\chi}{1 + \chi\ f_{v1}} . \tag{18}$$

The destruction term Y_υ is

$$Y_\upsilon = C_{w1}\ f_w \left(\frac{\tilde{\upsilon}}{d}\right)^2 \quad ; \quad f_w = g\left[\frac{1 + C_{w3}^6}{g^6 + C_{w3}^6}\right]^{1/6} \quad ; \quad g = r + C_{w2}\ (r^6 - r) \quad ; \quad r = \frac{\tilde{\upsilon}}{\tilde{\Omega}\ \kappa^2 d^2} \tag{19}$$

The empiric constants of the model are: C_{b1}=0.1355; C_{b2}=0.622; C_{w1}= $C_{b1} / \kappa^2 + (1 + C_{b2}) / \sigma_{\tilde{v}}$; C_{w2}=0.3; C_{w3}=2.0; $C_{\upsilon l}$=7.1; $\sigma_{\tilde{v}}$ =2/3; k=0.41.

3. RESULTS

The thin flat plate proposed by Crompton (2000) was modeled with the geometry described in Fig. 2. The plate has a chord length c of 160 mm and a span of 800 mm giving an aspect ratio of 5, which is sufficient to supply nominally two-dimensional flow.

The reattachment length was found by Crompton (2000) to be independent of **Re** above 10^5, where **Re** is defined as **Re**= $U_\infty\ c\ /\upsilon$, where U_∞ is the free stream velocity, and c the chord length. The wind tunnel investigation was carried at **Re** = 2.13×10^5 and this Reynolds number is used to compare the turbulence models and the experiments. Attack angles, α = 1 to 5 degrees, are available in experimental data in 1 degree intervals. At inclination of 5 degrees the flow

is separated for the majority of the length of the plate. The LDV measurements for the mean velocity and a few turbulent quantities over the plate are available at Crompton´s study (2000).

Figure 3 shows the computational domain used in simulations, which was defined based on the work of Collie (2005). At the inlet, the cartesian components of velocity are set according to the angle of attack and the turbulence intensity of the freestream defined as

$$\zeta = \frac{1}{3}\frac{(\overline{u'u'} + \overline{v'v'} + \overline{w'w'})}{U_\infty^2} = \frac{2}{3}\frac{\kappa}{U_\infty^2} \tag{20}$$

is set as 0.05%, as measured in wind tunnel (Crompton, 2000). Constant pressure equal to the freestream p_∞ was set at the outlet.

Figure 2. Thin flat plate dimensions.

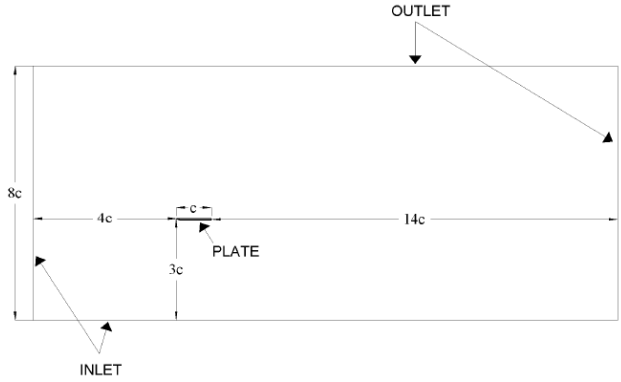

Figure 3. Domain details.

The mesh was created in the software GAMBIT with 3.5×10^5 cells, a slightly larger number of points than employed by Collie (2005), based on a grid convergence study performed by him. The distance of first node above the plate was designed as 6.25×10^{-5} c (c is the length of the chord) to guarantee $y^+=(\tau_s/\rho)^{0.5}\, y/\upsilon$ around 1, which is the value indicated for both RANS, where τ_s is the wall shear stress.

To flow field was determined with the commercial software Fluent (2006) with both models described in section 2. This code is based in Finite Volume Method. The QUICK scheme (Leonard, 1979) scheme was employed to discretize the governing equations. The pressure-velocity coupling was handled by the SIMPLE algorithm. The system of algebraic equation was solved with the Multgrid method (Hutchinson and Raithby, 1986). The problem was considered converged when the maximum residue of all equations was smaller than 10^{-6}.

3.1. Mean velocities profiles

Due to the abrupt geometry at the main extremity, a long and thin bubble is created at the leading edged just after the separation of the boundary layer. If the inclination angle is positive, the stagnation point will be located below the surface of the plate and due to the high inertial forces (high Reynolds number) the particles do not follow the abrupt curvature of the extremity and separation occurs. The separated shear layer is unstable and transition rapidly occurs. After transition, a rapid development of the shear layer occurs due the high rate of turbulence entrainment, which bends the streamlines toward the surface of the plate at the reattachment point X_R. Now, due to the favorable pressure gradient existent between the larger pressure point in the reattachment point and the minimum pressure point close to the bubble center, the portion of the flow that goes back to the leading edge suffers a relaminarization process. The boundary layer of this portion of the flow moves forward to the leading edge becoming again laminar and ready to suffer a second separation, generating a secondary recirculation bubble, since there is another adverse pressure gradient at the minimum pressure point in the center of the bubble to the leading edge. This second very small bubble is very hard to be predicted, and it was not observed with all RANS models.

Table 3 presents the reattachment lengths (X_R) for the flat plate at 1^o, 3^o and 5^o incidence angles, obtained by the present work. The results obtained by Collie (2005) with the κ–ω and SST models employing the CFX software (Ansys, 2007) are also presented. Sampaio et al (2006a) investigated the same problem for θ $=1^o$ with the LES methodology. The results obtained with the Smagorinsky Sub-Grid model are also included in Table 3.

The numerical prediction of the reattachment lengths obtained with the different turbulence models presented in Tab. 3 are approximately the same for all RANS models, with the exception of the κ–ω model, for θ $=1^o$. The SST, which is formed by a blending of the κ–ω model with the κ–ε model, predicted a better result. The present SST model predictions differ from Collie's results of approximately 2%, due to small differences in the mesh definition, as well as softwares implementations. For the inclination angle equal to 1^o, the LES methodology was able to predict a reattachment length with excellent agreement with experimental data (Sampaio et al, 2006a). The prediction of the

reattachment length with the Spalart-Allmaras model (SA), which requires less computational effort was quite good, specially for the greater angles of attach. It should be noticed that for smaller angles of attach; the bubble is smaller and therefore much harder to be predicted, leading to larger errors in relation to the experimental values.

Table 3 – Normalized reattachment lengths (X_R) and respective errors.

	X_R / c (θ =1°)	error	X_R / c (θ =3°)	error	X_R / c (θ =5°)	error
Experimental Crompton (2000)	0.140		0.470		0.942	
SA	0.153	9.2 %	0.462	1.6 %	0.929	1.4 %
SST	0.147	5.4 %	0.463	1.5 %	0.924	1.9 %
κ–ω (Collie, 2005)	0.184	24 %	0.510	8.4 %	-	-
SST (Collie, 2005)	0.149	5.8 %	0.437	6.4 %	-	-
Sampaio et al.(2006a)	0.139	0.4%	-	-	-	-

The mean velocities profiles obtained with SST and Spalart-Allmaras (SA) models for the incidence angles θ = 1° , 3° and 5° are compared with the experimental data de Crompton (2000) at three stations in Figs. 4, 5 and 6, respectively. All stations are located inside the bubble for θ = 3° and 5°, but for θ = 1° the third station is outside the bubble. The results obtained with the SST model by Collie (2005) were very similar to the present SST results and are omitted for clarity reason. For the θ=1° case, the LES results (Sampaio et al, 2006a) are also included in Fig. 4.

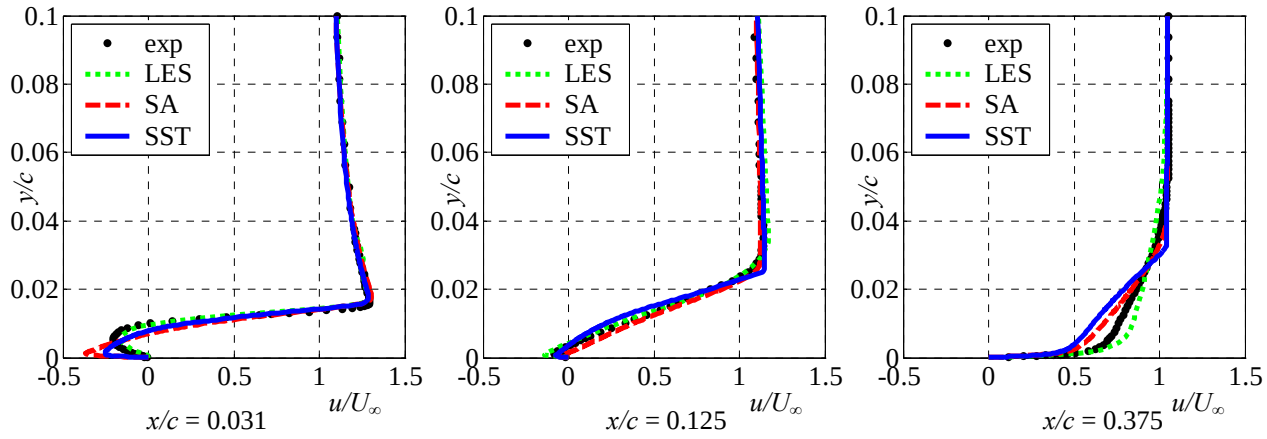

Figure 4. Velocities profiles for incidence angle θ =1° .

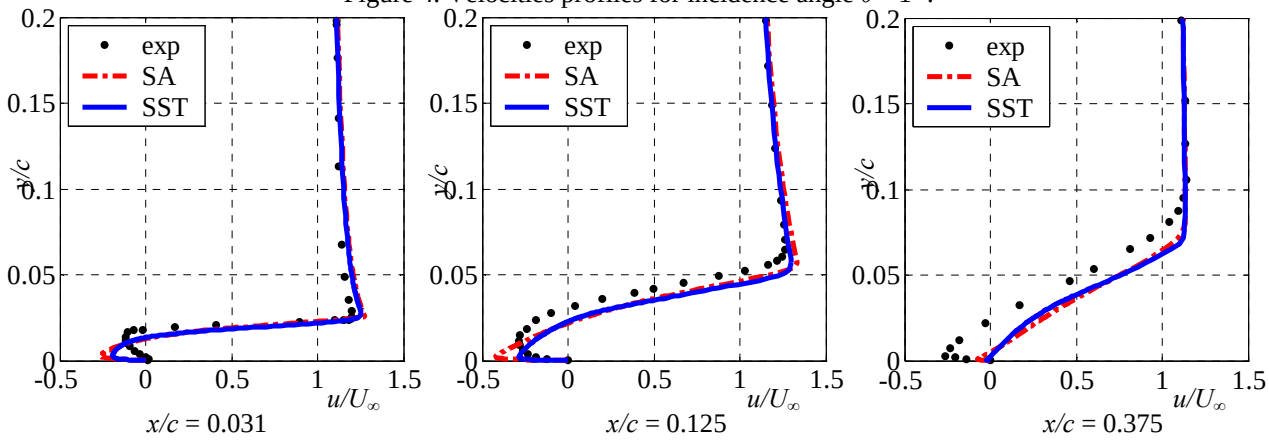

Figure 5. Velocities profiles for incidence angle θ =3°.

The reversed flow in the leading edge bubble experiences relaminarisation and the boundary layer begins to show very laminar features. The velocity profiles, in the two initial stations (x/c = 0.031 ; 0.125) of Fig. 4 and in all other stations of Figs. 5 and 6, which are inside the bubble, show that the experimental data has a more laminar profile in comparison with the RANS turbulence models results which all experience a sharp increase in velocity over the near-wall region, specially the SA model. To simulate the process of relaminarization an appropriate transition model is required which is not provided by the RANS models investigated, consequently these models predict greater velocity gradient in this wall region. On the other hand, for the θ=1° case, the LES results (Sampaio et al, 2006a) showed an

excellent agreement with experimental data for the two first stations inside the bubble (Figs. 4a and b). However, the agreement deteriorates at station 3, outside the bubble (Fig. 4c), where the velocity recovery is slower, while the RANS models predict a faster recovery. Collie (2005) attributes this difference between the turbulence models and experimental results to the influence of wind tunnel in the boundary layer, however, this assessment is difficult to quantify. Sampaio et al (2006a) attributed the discrepancy the LES model with the experimental data at this station to the mesh refinement. The present paper prefers to explain the discrepancies of the RANS models to their inability to capture the anisotropy of flow near the wall.

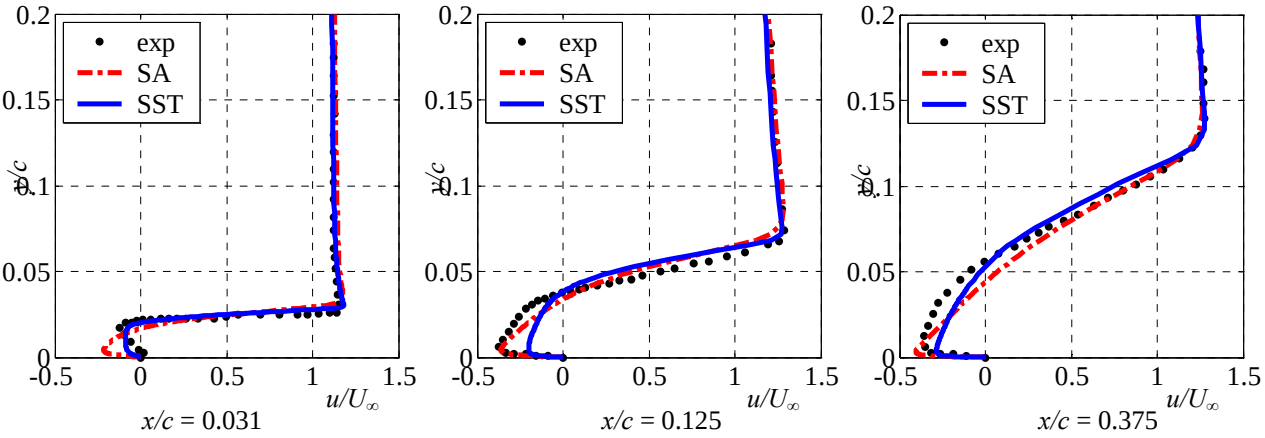

Figure 6. Velocities profiles for incidence angle θ =5^o .

After the reattachment point, the boundary layer continues to grow and developed turbulence is obtained. Normalizing the velocity u with the friction velocity $u_\tau = (\tau_s/\rho)^{0.5}$ ($u^+ = u/u_\tau$) and using a log scale for $y^+ = u_\tau y/\upsilon$, the boundary layer profiles at x/c = 0.875 for θ=1^o case are presented in Fig. 7. It can be seen that good results were obtained at this station, since both models agreed with the developed turbulence results in the sublayer and in the log-region.

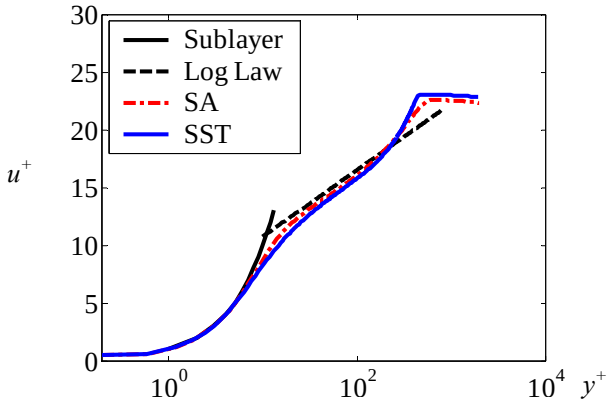

Figure 7. Velocity profile at x/c = 0.875 for angle of attack 1^o.

3.2. Pressure Distributions

The pressure distribution is analyzed through the pressure coefficient defined as

$$C_P = (p_\infty - p)/(0.5\ \rho\ U_\infty^2) \tag{21}$$

where p is the static pressure, p_∞ and U_∞ are the freestream pressure and velocity.

Figure 8 presents the variation of the pressure coefficient along the plate for θ =1^o. Again the RANS models SA and SST are compared with the experimental data. These results confirm the discussion of the previous section, i.e., the turbulence models overpredict the velocity magnitude near the wall, therefore, as expected the pressure distribution is underpredict. In Figure 8, the LES results of Sampaio et al. (2006) were also included. It can be seen a pressure peak displaced from the leading edge as the experimental data, however the pressure peak was also underpredicted as the RANS results. Further, the pressure coefficient drop of LES is steeper and delayed, in relation to the experimental data. Both RANS models underpredicted the pressure coefficient downstream of the reattachment point, where the LES results for θ=1^o was quite good.

Figure 9 illustrates the pressure coefficient for the three angles of attach along the plate, normalized by the reattachment point, x/X_R. It can be observed that near the leading edge, where the separation occurs for all cases, the maximum pressure is near one. It can also be clearly seen the similarity of the flow for the different angles, once all experimental data are very close together. The SA model is capable of capturing this similarity, however for the SST model, a smaller C_P peek is predicted for θ=5°.

In the interior of the thin airfoil bubble the pressure is mainly determined by the shear layer curvature, in other words, stronger streamline curvature will lead to smaller pressure. Due to the difficulty of the turbulence models to predict with accuracy the transition position and resolution of the secondary bubble, these models demonstrate an inferior and flatter suction peak. Larger discrepancies between the predictions and the experimental data are observed as the angle of attack increases. These discrepancies are associated with the inability of the models to predict the complex flow inside the bubble. Large angles of attack are associated with longer bubbles; therefore, worse predictions are obtained. These results encourage the investigation of these higher angles with LES, in spite of being much more expensive.

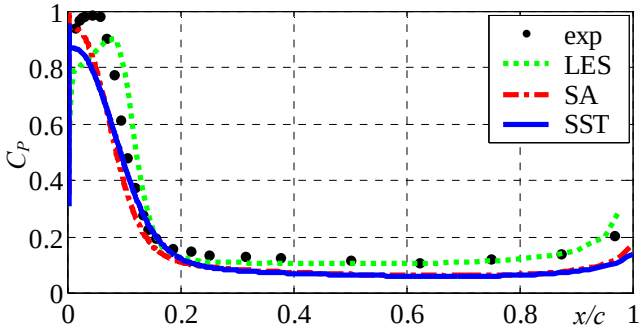

Figure 8. Pressure Coefficient for angle of attack 1°

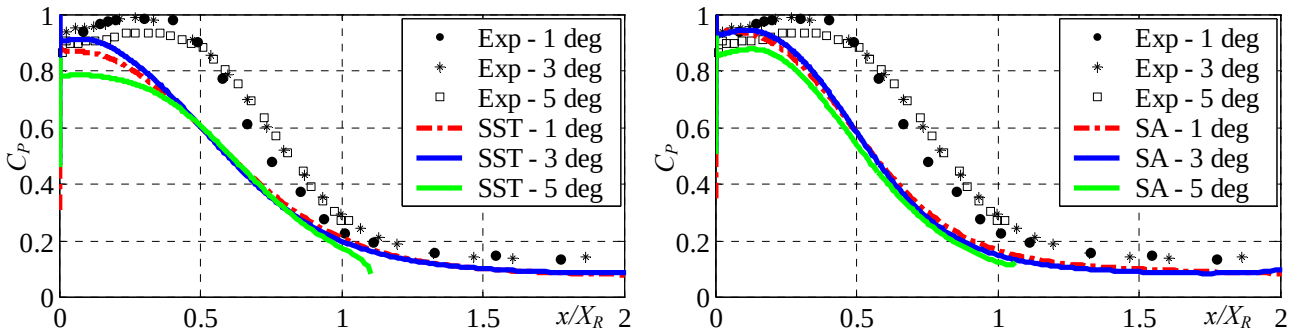

(b) SST pressure coefficient for 1°, 3° and 5°

(c)SA pressure coefficient for 1°, 3° and 5°

Figure 9. Pressure Coefficient for angle of attack 1°, 3° and 5°

3.3. Second order statistics

The turbulent second order statistics $\overline{u'u'}$ predicted with SA and SST are compared with the experimental data in Figs. 10, 11 and 12 for the three angles of incidence. For θ=1°, the LES results of Sampaio et al (2006) are also included in Fig. 10, where it can be seen that at the first station the production of turbulence is underpredicted resulting in smaller $\overline{u'u'}$, being overpredicted at x/c=0.125, what is in agreement with the displaced pressure peak observed in Fig 8a. After the reattachment point, its predictions are superior to the RANS predictions.

The Spalart-Allmaras model uses a viscous damping function to better represent the buffer layer and viscous sublayer, but this feature results in a major damping of entrainment rate and consequently smaller turbulence levels inside the bubble, which are visible in all stations for the three cases shown in Figs. 10, 11 and 12.

The SST model simulates more turbulence in the shear layer than the Spalart-Allmaras model. For turbulent boundary layers the SST model uses standard κ–ω in the near-wall region and then blends to the standard κ–ε model across the outer region of boundary layer. Nevertheless inside the thin airfoil bubble the SST model blends κ–ε across the inner region of the bubble so that the ε–equation is solved across the shear layer. Therefore it appears that the ε–equation predicts a lower dissipation of turbulence which leads an over prediction of turbulence in the separated shear layer. Thus the increase of turbulence is a direct result of the ε–equation which actually improves SST results. This

effect is partially compensating for the model's inability to predict the increase in the turbulence entrainment.

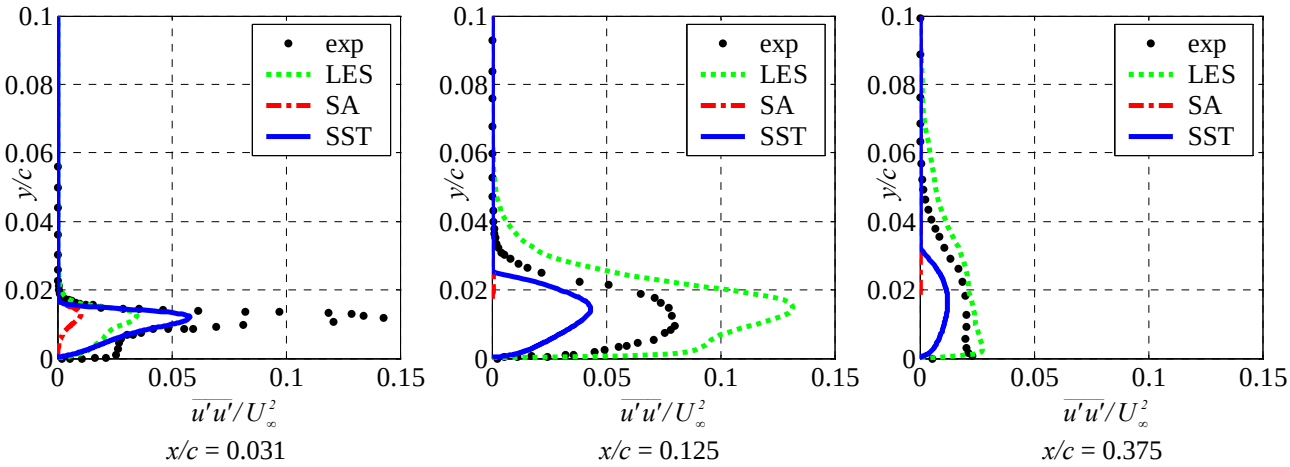

Figure 10. Second order statistics for angle of attack 1° .

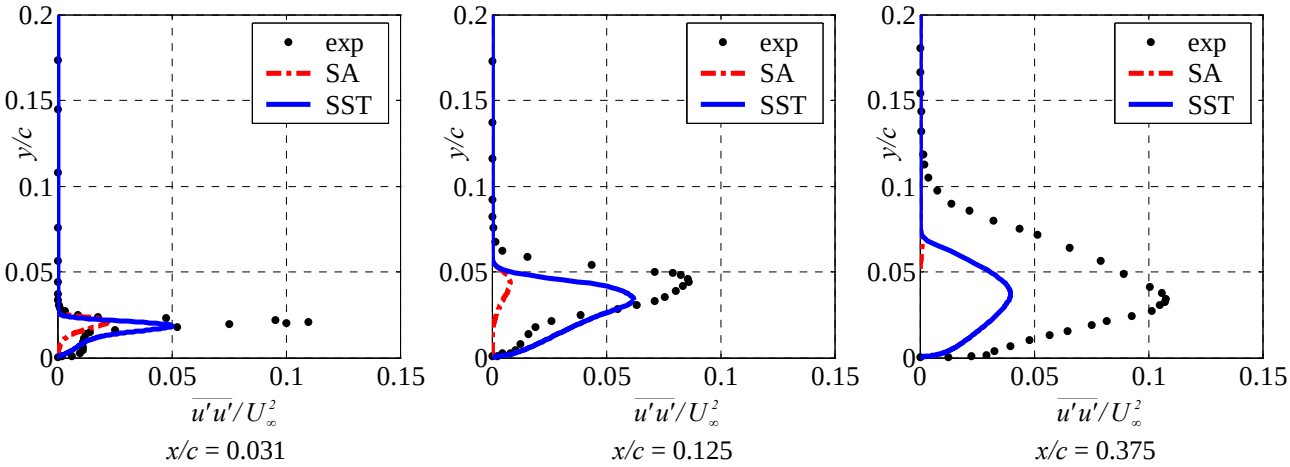

Figure 11. Second order statistics for angle of attack 3° .

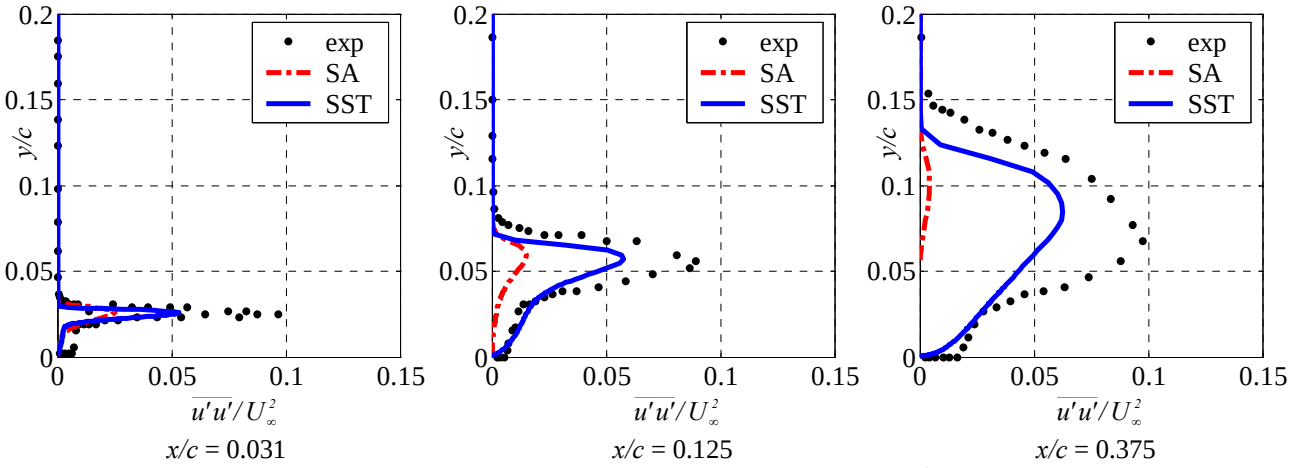

Figure 12. Second order statistics for angle of attack 5° .

4. CONCLUSION

In the present work, the turbulence models of Spalart-Allmaras (1992) and SST (Menter, 1994) were applied to determine the incompressible flow over a flat plate with a sharp leading edge, with small inclination angles. Three different angles were investigated θ =1°, 3° and 5°. The results obtained were compared with experimental data of Crompton (2000). For θ=1° the solution was also compared with available LES results (Sampaio, 2006).

The mean profiles velocities presented reasonable agreement with the experimental results; however the details of

the recirculating bubble were underpredicted in size and over predicted in magnitude. Qualitatively the profiles are the same for the different angles of attach indicating the presence of similarity. The prediction of the reattachment length was improved with the increase of the angle of attack; on the other hand, the pressure distribution over the plate has deteriorated. The LES model prediction was slightly superior in relation to the pressure distribution for $\theta=1^o$, as well as the second order statistics. Although a better prediction of the reattachment length was obtained with the SA model, the overall results of the SST were better. The difficulty to capture the entrainment of the separated shear layer, encourage the investigation of the problem with more demanding models such as LES and DNS.

5. ACKNOWLEDGEMENTS

The authors acknowledge the support awarded to this research by the Brazilian Research Council, CNPq.

6. REFERENCES

ANSYS CFX-Solver Theory Guide, v. 10, 2006, Ansys INc.

Cazalbou, J.B., Spalart, P.R., Bradshaw, P., 1993, "On the Behavior of 2-Equation Models at the Edge of a Turbulent Region", Physics of Fluids, Vol. 6, No. 5, pp. 1797-1804.

Collie, S., 2005, "Application of CFD to Two-Dimensional Downwind Sail Flows", PhD Thesis, Department of Mechanical Engineering Science of the University of Auckland, New Zealand.

Crompton, M. J.; Barret, R. V., 2000, "Investigation of the Separation Bubble Formed Behind the Sharp Leading Edge of a Flat Plate at Incidence". Proceedings of the Institution of Mechanical Engineers Part G-Journal of Aerospace Engineering, Vol. 214, No. G3, pp. 157-176.

Crompton, M., 2001, "The Thin Airfoil Leading Edge Separation Bubble", PhD Thesis, Department of Aerospace Engineering University of Bristol.

Cyr S, Newman BG, 1996, "Flow past two-dimensional membrane aerofoils with rear separation", Journal Of Wind Engineering And Industrial Aerodynamics, Vol. 63 (1-3): Pp.1-16.

Dacles-Mariani, J., Zilliac, G. G, Bradshaw, P., Chow, J. S, 1995, "Numerical/Experimental Study of a Wingtip Vortex in the Near Field", AIAA Journal, Vol. 33, No. 9, pp. 1561-1568.

Deck, S., Duveau, P., D'Espiney, P., Guillen, P., 2002, "Development and Application of Spalart-Allmaras One Equation Turbulence Model to Three-Dimensional Supersonic Complex Configurations", Aerospace Science and Technology, Vol. 6, No. 3, pp. 171-183.

Fluent User's Guide, v. 6.2, 2006, Fluent Inc., New Hampshire.

Gault, D. E., 1957, An investigation at low speed of the _ow over a simulated _at plate at small angles of attack using pitot static and hot-wire probes, Technical Report TN-3876, NACA.

Hutchinson, B. R., and Raithby, G.D., 1986, "A Multgrid Method Based on the Additive Correction Strategy", Numerical Heat Transfer, vol. 9, pp.511-537.

Leonard, B.P. 1979, "A Stable Accurate Convective Modeling Procedure Based on Quadratic Upstream Interpolation", Computer Methods in Appied. Mechanics and Engineering, Vol.19, pp. 59-88.

Lian YS, Shyy W, 2005, "Numerical simulations of membrane wing aerodynamics for micro air vehicle applications", Journal Of Aircraft Vol. 42 (4): pp. 865-873.

Menter, F. R., 1992, "Influence of Freestream Values on k-ω Turbulence Model Predictions", AIAA Journal, Vol. 30, No. 6, pp. 1657-1659.

Menter, F. R., 1994, "Two-Equation Eddy-Viscosity Turbulence Models for Engineering Applications", AIAA Jounal, Vol. 32, No. 8, pp. 1598-1605.

Menter, F. R., Kuntz, M., Langtry, R., 2003, "Ten Years of Industrial Experience with the SST Turbulence Model", Proceedings of the 4th International Symposium on Turbulence, Heat and Mass Transfer, pp. 625-632.

Newman Bg, Tse Mc, 1992, "Incompressible-Flow Past A Flat-Plate Aerofoil With Leading-Edge Separation Bubble", Aeronautical Journal Vol. 96 (952), pp. 57-64.

Sampaio, L.E.B. Nieckele, A. O., Gerritsen, M. and Collie, S., 2006a, "Numerical Simulations Of The Long Recirculation Bubbles Formed In Incompressible Aerodynamic Flows Over Thin Flat Plates At Shallow Incidence", Proceedings of the 11th Brazilian Congress of Thermal Sciences and Engineering -- ENCIT 2006, Paper CIT06-0278

Sampaio, L.E.B. Nieckele, A. O., Gerritsen, M. and Collie, S., 2006b, "Large Eddy Simulations of the Long Recirculation Bubbles Formed in Thin Flat Plates at Shallow Incidence", Proceedngs of the 5th Spring School of Transition and Turtbulence, EPTT2006, Paper ETT06-15.

Spalart, P., Allmaras, S., 1992, "A one-equation turbulence model for aerodynamic flows", Technical Report AIAA-92-0439, American Institute of Aeronautics and Astronautics.

7. RESPONSIBILITY NOTICE

The authors are the only responsible for the printed material included in this paper.